Ref: 641-607
Job Order 75-215
NAS 9-12200

NASA CR-

TECHNICAL MEMORANDUM *141556*

SL-4 INTERIM REPORT

ANTENNA PERFORMANCE AND RESOLUTION

SPE-S194-005

By

J. J. Carney

Approved: _O. W. Brandt, Supervisor_
Exploratory Investigations

November 1974   LEC-4946

7. ANTENNA PERFORMANCE AND RESOLUTION (SPE-S194-005 S & AD)

The purpose of this task is to verify the performance of the antenna throughout SL-2, SL-3, and SL-4. Also, determine the antenna resolution of brightness temperatures under actual flight conditions.

The approach to determine antenna performance was to have the field of view of the antenna traverse a land/water interface. The water will provide a low, essentially homogeneous brightness temperature target. The land is chosen so as to be essentially homogeneous and of a high brightness temperature (desert). The site chosen was simulated by a digital computer program along with a model of the sensor and the antenna gain patterns acquired from acceptance tests. The results of these simulations will be the baseline to which flight data throughout the Skylab flight will be compared and evaluated.

The approach to determine antenna brightness temperature resolution will be to utilize the land/water interface flight data to arrive at a figure of merit for the resolution of the antenna. This figure of merit will be the minimum change in brightness temperature of the target per unit area within the target that is detectable by the antenna. This value will aid in the evaluation of data acquired over sites of a non-homogeneous nature and also provide a baseline for future instruments.

7.1 Target Site Selection

Table 7.1-1 lists the target site selected for the execution of this task, utilizing SL-2, SL-3, and SL-4 flight data. A single target site was selected for this task due to the unique sensor response for this site being especially useful to determine the performance and resolution of the antenna. The site chosen will produce essentially a triangular response curve with the nearly homogeneous land area producing the peak signal and the two bodies of water (Pacific Ocean and Gulf of California) producing the baseline of the triangular pulse. Different ascending ground tracks across Baja California will produce different widths for the triangular pulse; however, the width change is directly relatable to the width of the land area traversed. Also, atmospheric effects on the brightness temperature will be slight at the latitudes involved. EREP data passes must be ascending so as to provide the correct intersection with the land/water interfaces.

TABLE 7.1-1. — TARGET SITE FOR ANTENNA PERFORMANCE AND RESOLUTION

Site number	Name	Coordinates latitude — longitude	Target characteristics	Skylab pass number		
				SL-2	SL-3	SL-4
750183	Baja, California	21°30'N, 111°30'W 25°30'N, 106°00'W 29°00'N, 118°30'W 33°00'N, 112°30'W	No rain over target. Ascending pass is required.	No data acquired	27 28 38 45	81 82

7.2   Land/Water Interface Simulations

The simulation of a land/water interface target involves the modeling of an essentially homogeneous target (water) and a non-homogeneous target (land). The following will describe in detail the models developed for the land/water interface simulation.

7.2.1   Target Geometry

The radiometric scene to be modeled is first partitioned into some convenient number of closed contours. The areas within these contours represent locations of constant brightness temperature. The contours defining the target are then approximated by a series of straight line segments. The position of the end points of these line segments are required to model the target. The coordinate system in which these line segments are defined may be arbitrarily chosen by the user and shall be referred to as the S system. In addition to the above information the radiometric temperature associated with each contour is also input to the program.

The number and complexity of the contours defining the target scene depends on the amount of digital computer core storage available, and the degree of resolution required of the scene. However, an input of twenty closed contours of thirty sides each is easily accomplished on a machine with 64 K storage.

After reading the contour and radiometric temperature data, the program overlays a grid of horizontal lines on the target. Solutions are then computed for the intersections of the horizontal grid lines with the line segments defining the contours, (Figure 7.2.1-1). The solutions of these linear equations are then used to build up a matrix which contains the digitized radiometric target. This process of solving for intersections of line segments is then repeated for each contour.

The errors inherent in the digitization of the target vary with the geometric shape of the target and the amount of computer storage available. Using a digitized scene of 100 by 120 locations and regularly shaped contours typical errors in the areas constructed by this process are less than one-half of one percent.
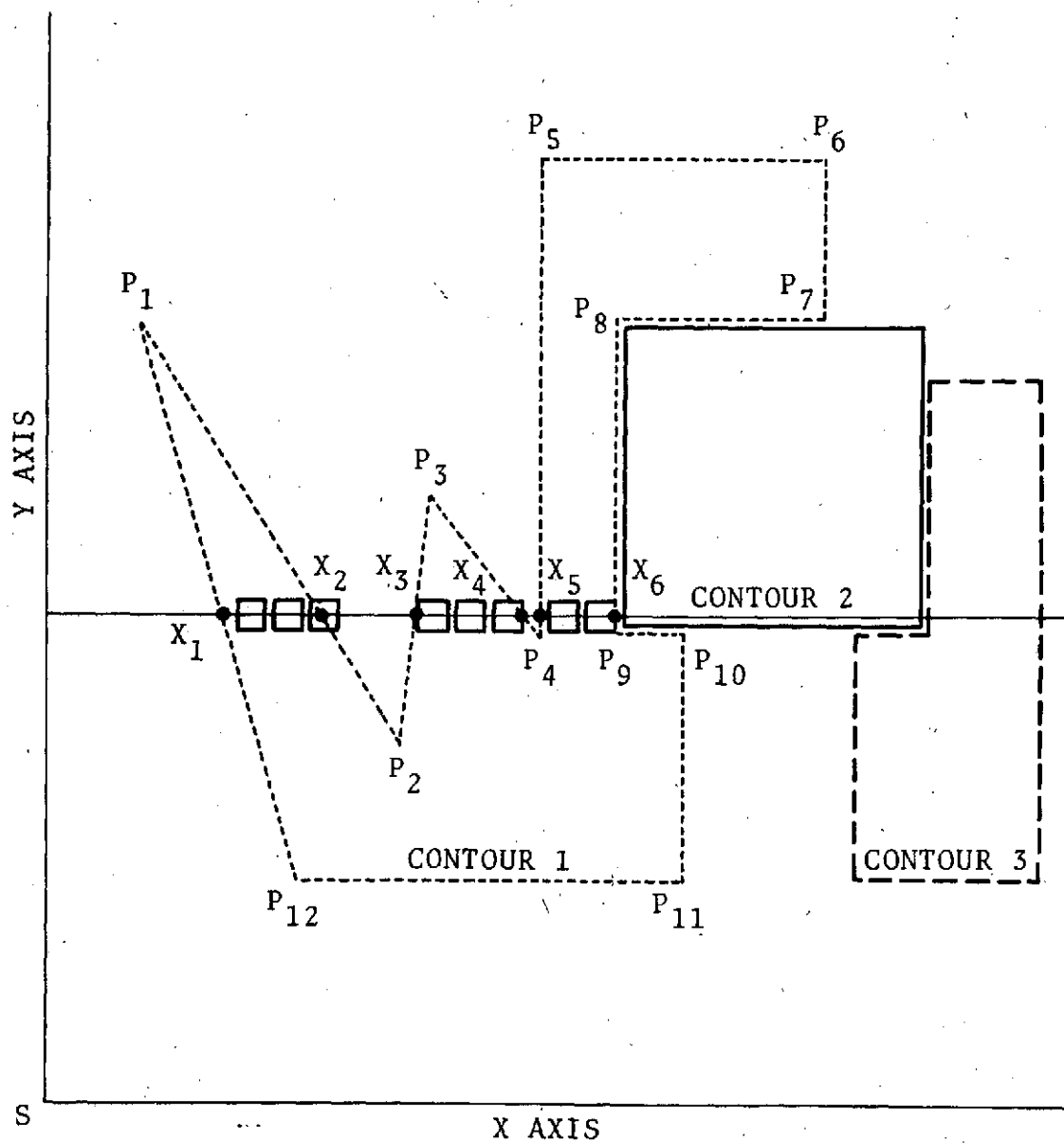
Figure 7.2.1-1. — Construction of simulated radiometric scene.

7.2.2 Coordinate Transformations and Antenna Orientation

The specification of antenna position and attitude requires the use of several coordinate systems. The system in which the radiometric target is defined is labeled the S system. The matrix containing the antenna gain pattern information is defined in the S''' system. This system has some given position and attitude with respect to the S system. To obtain the desired radiometric brightness temperature for the target an integration of the target brightness over the antenna gain pattern must be performed. This integration requires the use of the transformation equations between the S and S''' systems.

To obtain the transformation equations between the S and S''' systems two intermediate coordinate systems, S' and S'' will be defined. The S' system has its Cartesian axes parallel to those of the S , but has its origin displaced by the Cartesian coordinates α_0, β_0, γ_0 . Hence the transformation equations between S and S' are:

$$\begin{bmatrix} x' \\ y' \\ z' \end{bmatrix} = \begin{bmatrix} x \\ y \\ z \end{bmatrix} - \begin{bmatrix} \alpha_0 \\ \beta_0 \\ \gamma_0 \end{bmatrix}$$

Equation
7.2.2-1

where x, y, z are the coordinates of some arbitrary increment of area Δa in the S system and x', y', z' are the coordinates of the same increment in the S' system. Two rotations are now performed on the S' system. First the S' system is rotated in a counterclockwise sense about the z axis through an angle Φ thus giving the S'' system. The transformation from S' to S'' is given by:

$$\begin{bmatrix} x'' \\ y'' \\ z'' \end{bmatrix} = \begin{bmatrix} \cos\Phi & \sin\Phi & 0 \\ -\sin\Phi & \cos\Phi & 0 \\ 0 & 0 & 1 \end{bmatrix} \begin{bmatrix} x' \\ y' \\ z' \end{bmatrix}$$

Equation
7.2.2-2

where x'', y'', z'' are the Cartesian coordinates of the previously defined differential of area in the S'' system.

Finally the S'' system is rotated in a counterclockwise sense about the x axis through the angle Θ (Figure 7.2.2-1). The transformation from S'' to S''' is given by:

$$
\begin{bmatrix} x''' \\ y''' \\ z''' \end{bmatrix} = \begin{bmatrix} 1 & 0 & 0 \\ 0 & \cos\Theta & \sin\Theta \\ 0 & -\sin\Theta & \cos\Theta \end{bmatrix} \begin{bmatrix} x'' \\ y'' \\ z'' \end{bmatrix} \qquad \text{Equation } 7.2.2-3
$$

A set of spherical coordinates is now defined (Figure 7.2.2-2) with respect to the Cartesian axes of S''' as follows:

$$
\begin{aligned}
x''' &= R''' \; \sin\theta \; \cos\phi \\
y''' &= R''' \; \sin\theta \; \sin\phi \\
z''' &= R''' \; \cos\theta
\end{aligned}
\qquad \text{Equation } 7.2.2-4
$$

where R''' is the distance from the origin of S''' to the differential of area Δa, and θ and ϕ are defined in the usual way.

The antenna gain pattern may either be hard coded into the program or read in from cards. Data is arranged so that the maximum gain direction is pointed down the $-Z$ axis of the S''' system. Hence by adjusting the parameters α_0, β_0, γ_0, Θ, ϕ, the position and attitude of the antenna may be adjusted for the required simulation.

The resolution of the antenna gain pattern is dependent on the electronic storage available and may be considerably improved by the use of data packing. For this application increments of five degrees in both θ and ϕ were used.
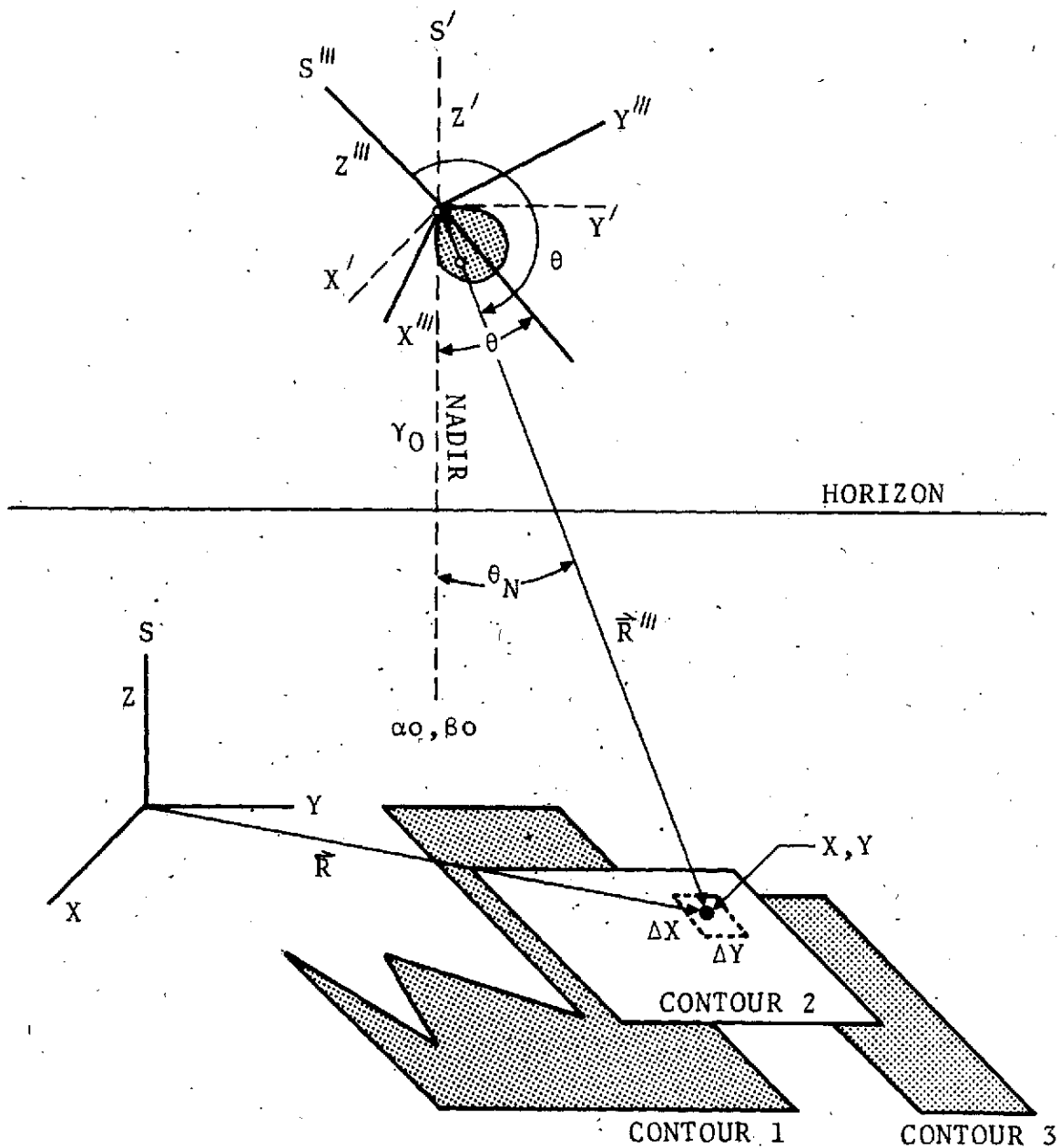
Figure 7.2.2-1. — Orientation of antenna coordinate system (S''') with respect to radiometric target system (S).
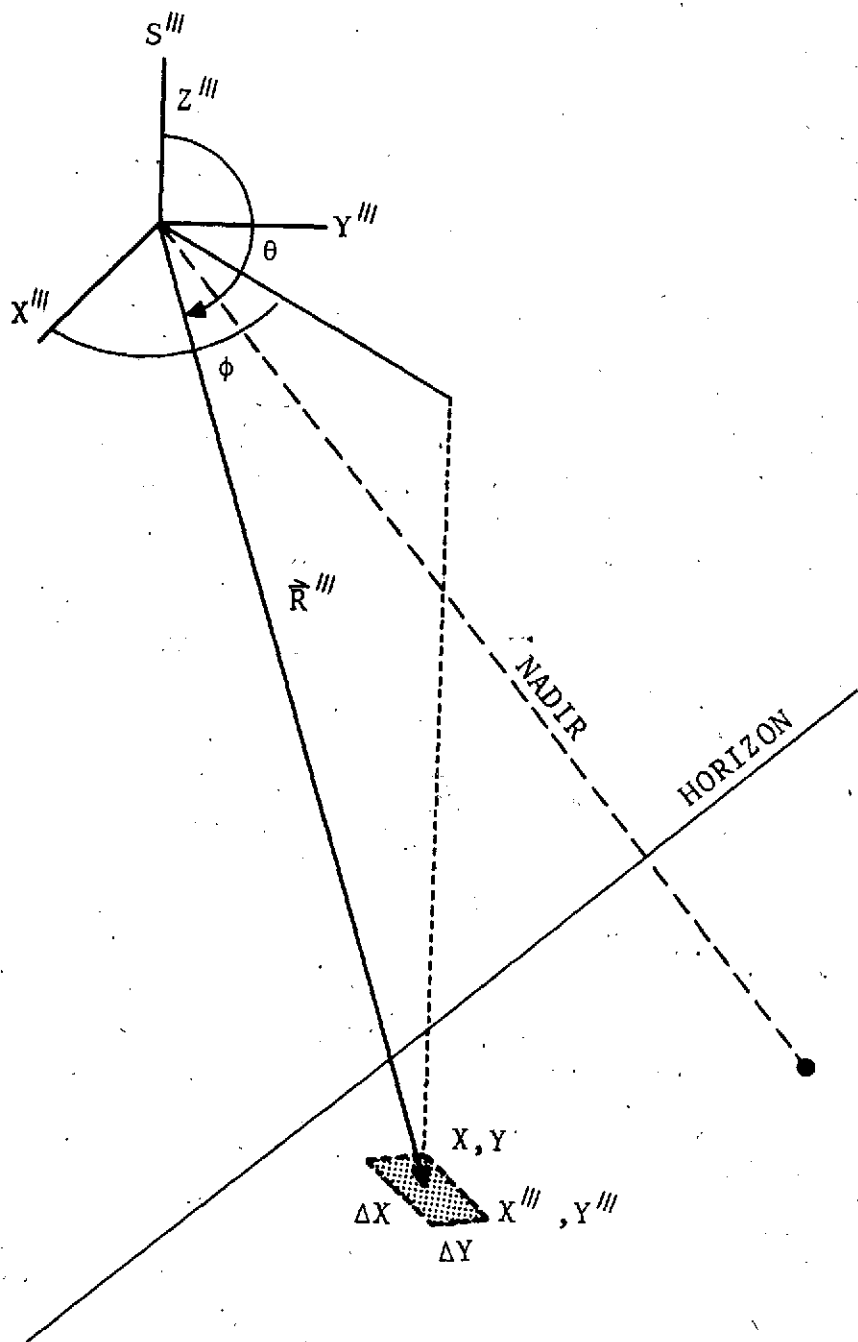
Figure 7.2.2-2. — Definition of angles in antenna coordinate system.

7.2.3 Integration Over Radiometric Target

The digital computer program computes the brightness temperature, B, for a simulated target. This quantity is defined as follows:

$$B = \frac{\int A(\theta,\phi)T(\theta,\phi)\ d\Omega}{\int A(\theta,\phi)\ d\Omega}$$

Equation 7.2.3-1

where A is the antenna gain function, T is the radiometric temperature function of the target, and $d\Omega$ is a differential of solid angle in the S''' system. The upper and lower integrals are performed over all solid angles. θ is the angle between the +Z axis of S''' and the vector $\vec{R}'''$, which goes from the origin of S''' to the arbitrary differential of area "da" whose coordinates are x and y in the S system. ϕ is the angle between the x axis of the S''' system and the projection of $\vec{R}'''$ into the X-Y plane of S'''. If R''' is much greater than dx or dy (Figure 7.2.2-1), then $d\Omega$ may be approximated by:

$$d\Omega \approx \frac{da\ \cos\theta_N}{\left(R'''\right)^2} \qquad da = dx\ dy$$

Equation 7.2.3-2

where θ_n is the angle between the nadir line from the origin of S''' and $\vec{R}'''$. θ_N is given by:

$$\cos\theta_N = \frac{Y_0}{R'''}$$

Equation 7.2.3-3

The upper integral of equation 7.2.3-1 may be approximated by a double sum extending over the target area as follows:

$$\int A(\theta,\phi)T(\theta,\phi) \ d\Omega \approx \sum_X \sum_Y \frac{T(x,y)A[\theta(x,y),\phi(x,y)] \ \cos \theta_N \Delta a}{R'''^2}$$

$$\Delta a = (\Delta x)(\Delta y)$$

Equation
7.2.3-4

where the double sum extends over all increments of area in the target. The antenna gain pattern values are stored in a two dimensional matrix array. The form of the expression of A, whose independent variables θ and ϕ are expressed as a function of x and y is necessary since the observation angles θ and ϕ must be computed as a function of the relative position of each Δa in the target. In this manner the required integral over solid angles is replaced by a double sum in the target plane. In computing the expression in the brackets in Equation 7.2.3-4 for each increment area, all quantities present are easily calculated except for the proper value of A. To compute this quantity, the angles that R''' makes with the S''' system must be calculated. Solving Equations 7.2.2-1 through 7.2.2-4 for θ and ϕ gives

$$\cos \theta = \frac{(x-\alpha_0) \sin \theta \sin \Phi - (y-\beta_0) \sin \Theta \cos \Phi + Z \cos \theta}{R'''}$$

Equation
7.2.3-5

$$\sin \phi = \frac{-(x-\alpha_0) \sin \Phi \cos \Theta + (y-\beta_0) \cos \Theta \cos \Phi + Z \sin \theta}{R''' \sin \theta}$$

Equation
7.2.3-6

where

$$R''' = [(x-\alpha_0)^2 + (y-\beta_0)^2 + (z-\gamma_0)^2]^{1/2}$$

Once θ and ϕ are computed, the corresponding value of A may be picked from the matrix containing the antenna gain values as a function of these two angles.

The lower integral of Equation 7.2.3-1 may be approximated and computed as follows:

$$\int A(\theta,\phi) \, d\Omega \approx \sum_\theta \sum_\phi A(\theta,\phi) \sin \theta \Delta\theta \Delta\phi$$

7.2.4 Flight Path Simulation

To simulate an aircraft or spacecraft flight path the previously described integrals are performed for successive values of the position and attitude parameters x_0, y_0, z_0, Θ_0, Φ_0 . Information defining the initial values of these parameters as well as the amounts by which they are to be incremented for each successive integration is read from cards. After each integration new values of position and attitude are computed as follows:

$$\alpha_i = \alpha_{i-1} + \Delta x$$

$$\beta_i = \beta_{i-1} + \Delta y$$

$$\gamma_i = \gamma_{i-1} + \Delta z$$

$$\Theta_i = \Theta_{i-1} + \Delta\Theta$$

$$\Phi_i = \Phi_{i-1} + \Delta\Phi$$

where

$$\alpha_1 = \alpha_0$$

$$\beta_1 = \beta_0$$

$$\gamma_1 = \gamma_0$$

$$\Theta_1 = \Theta_0$$

$$\Phi_1 = \Phi_0 \qquad i = 1, 2, \cdots \text{number of flight path configurations}$$

In this manner a flight path of any straight line and various antenna motions may be simulated. With slight alterations to the above equations completely general flight path configurations are possible.

7.2.5 Antenna Gain Patterns

The E-Plane and H-Plane gain patterns at the mid-band frequency of 1.400 GHz for S194 antenna unit number 001 are shown in Figures 7.2.5-1 and 7.2.5-2, respectively. These antenna gain patterns were acquired from preflight laboratory tests.

7.3 Antenna Performance from Land/Water Interface

Unfortunately no ascending EREP data passes were performed over Baja, California, during SL-2. There were four ascending EREP data passes performed over Baja, California, during SL-3, Skylab pass numbers 27, 28, 38, and 45. During SL-4 Skylab pass numbers 81 and 82 acquired data over this target site. The following sections will describe the results of the analysis of the above data.

7.3.1 SL-2 Antenna Performance from Land/Water Interface

Since no data was acquired over the selected target site, the following substitution will be made in order to arrive at an estimate of the antenna performance. The California coastline, intersected during EREP pass numbers 1 and 11, will be substituted for the Baja, California, site.
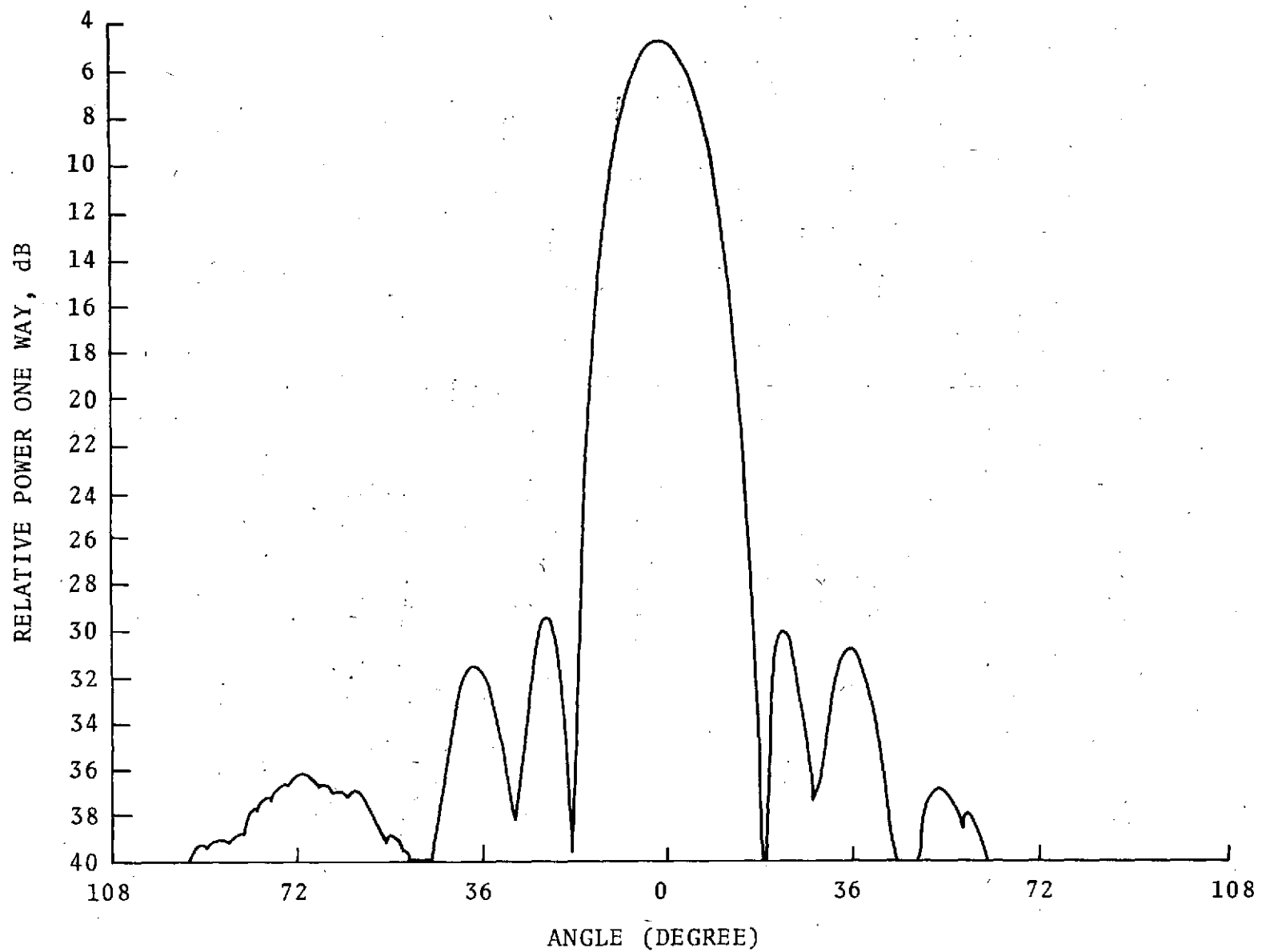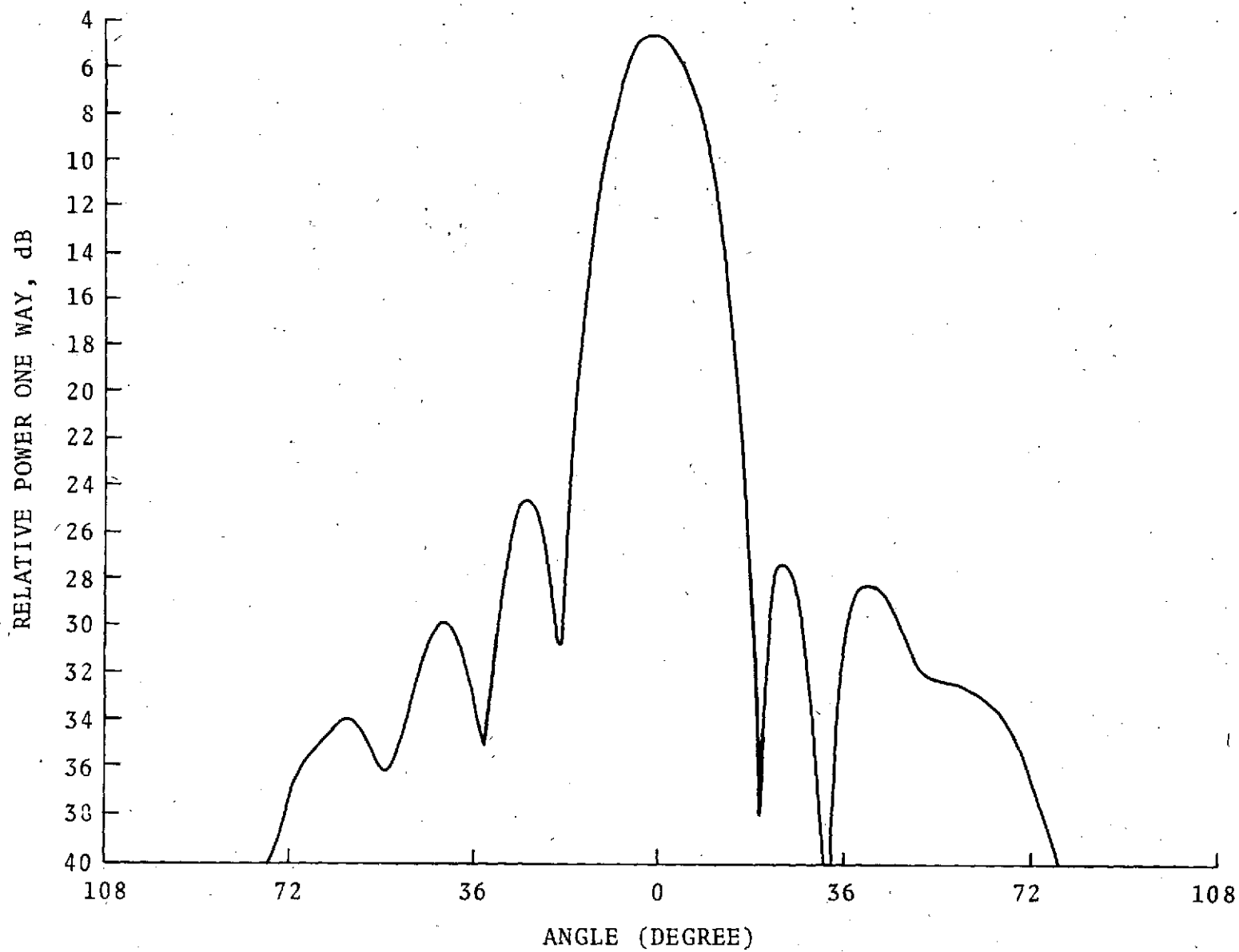
Figure 7.2.5-1. — S194 antenna pattern, E-plane.

Figure 7.2.5-2. — S194 antenna pattern, H-plane.

Table 7.3.1-1 lists the pertinent information for the two EREP data passes over this substitute target site for the land/water interface. Figures 7.3.1-1 and 7.3.1-2 show the response of the sensor (lower half of the figure) in reference to the position of the field of view on the earth's surface (upper half of the figure). Also, the relative size of the antenna pattern is indicated by the solid circle (3 dB points) and the dashed circle (null-to-null). The time (GMT) as shown along the abscissa of the lower half of each figure is not a linear function due to the orbit of the Skylab vehicle. The time values shown merely indicate the value of GMT when the center of the field of view of the sensor passed the indicated longitude on the earth's surface.

The relative land/water interface transitional response between Skylab pass numbers 1 and 11 will be evaluated by comparing the slopes and changes in slopes of the S194 response curves shown in Figures 7.3.1-1 and 7.3.1-2. Even though the base level and the peak values of brightness temperatures differ slightly, the transitional response between Skylab passes 1 and 11 is very similar and occurs within the same length of time. Thus, it may be concluded that during the approximately 15 days between Skylab pass numbers 1 and 11, no gross changes occurred in the antenna which would affect the antenna gain pattern and, consequently, the performance of the antenna.

7.3.2   SL-3 Antenna Performance from Land/Water Interface

Figures 7.3.2-1 through 7.3.2-3 are plots of the measured brightness temperature as the field of view of the S194 sensor traversed the Baja, California, target site during Skylab pass numbers 27, 28, and 38, respectively. The Baja, California, data acquired during Skylab pass number 45 will have to be reprocessed due to the fact that the internal calibration hot load had not reached the design level of 373°K before the calibration interval was initiated. Housekeeping data indicates that the hot load had a value of 355°K at the time of calibration. The postflight processing of the data utilized this incorrect value for the hot load and, therefore, reprocessing of the data using the trailing calibration values will have to be performed. Unfortunately, Skylab pass numbers 27 and 45 had the same ground track but comparison of data is not possible due to the reprocessing requirement on Skylab pass 45 data.

TABLE 7.3.1-1. — SUBSTITUTE TARGET SITE FOR THE LAND/WATER INTERFACE

Site name	GMT start: GMT stop:	Coordinates latitude - longitude	Target characteristics	SL-2 Skylab pass number
California coastline	150:20:37:50 150:20:38:20	Start: 43.9°N, 125.5°W Stop: 43°N, 123.3°W	No rain over target	1
California coastline	165:14:40:00 166:14:40:30	Start: 43.5°N, 124.7°W Stop: 42.6°N, 122.5°W	No rain over target	11

Figure 7.3.1-1. — Brightness temperature versus time and position.
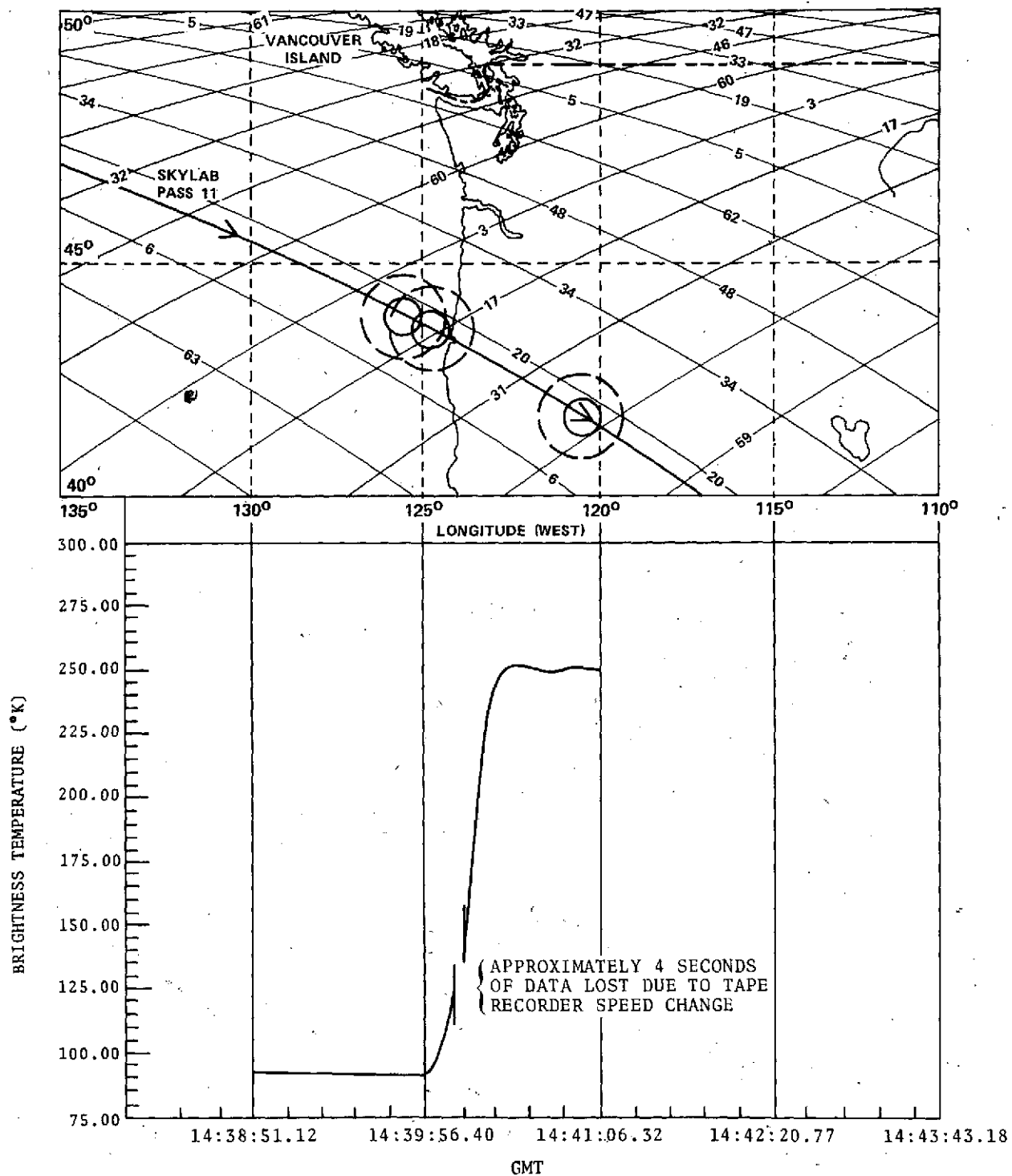
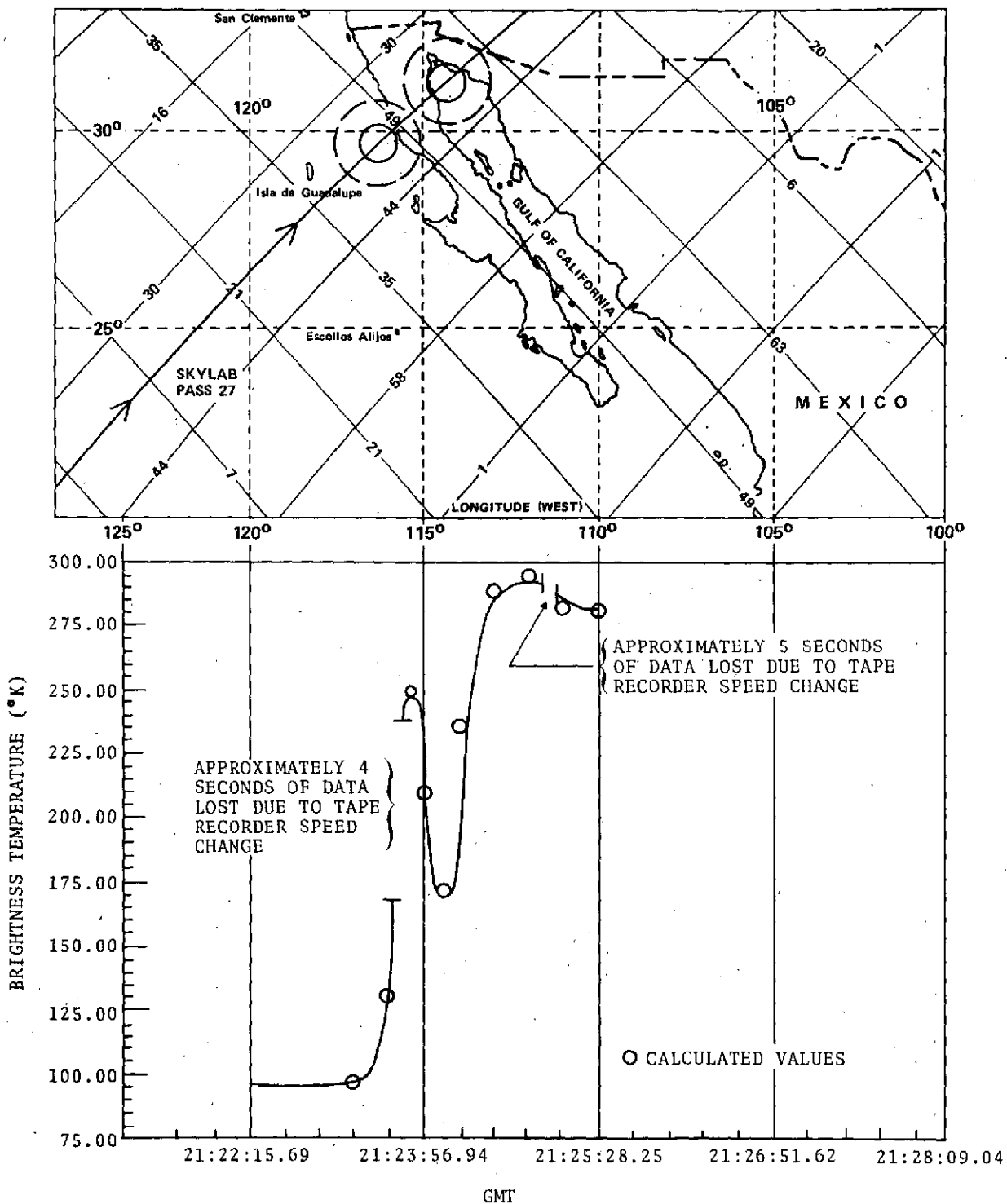Figure 7.3.1-2. — Brightness temperature versus time and position.

Figure 7.3.2-1. — Brightness temperature versus time and position.
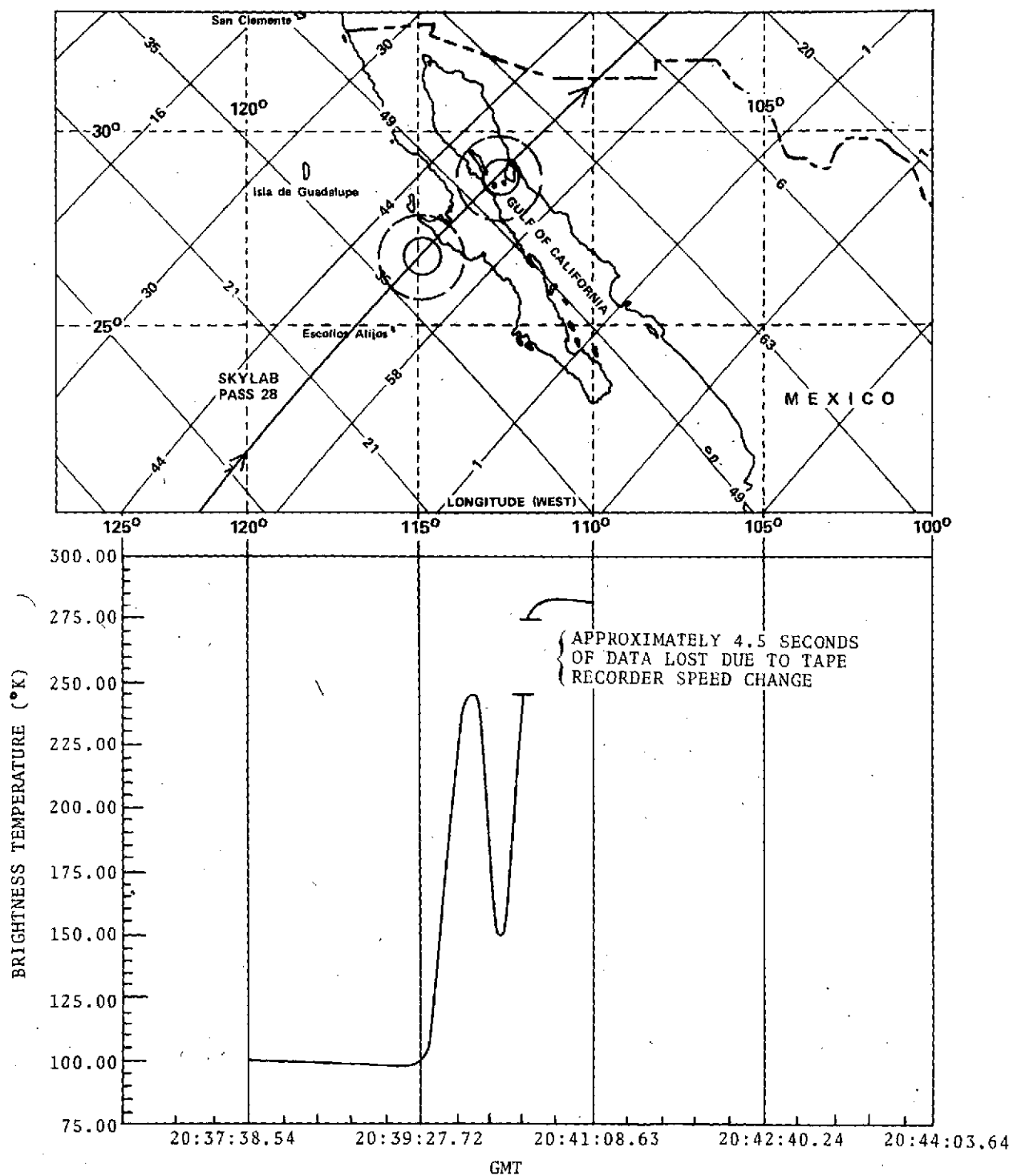
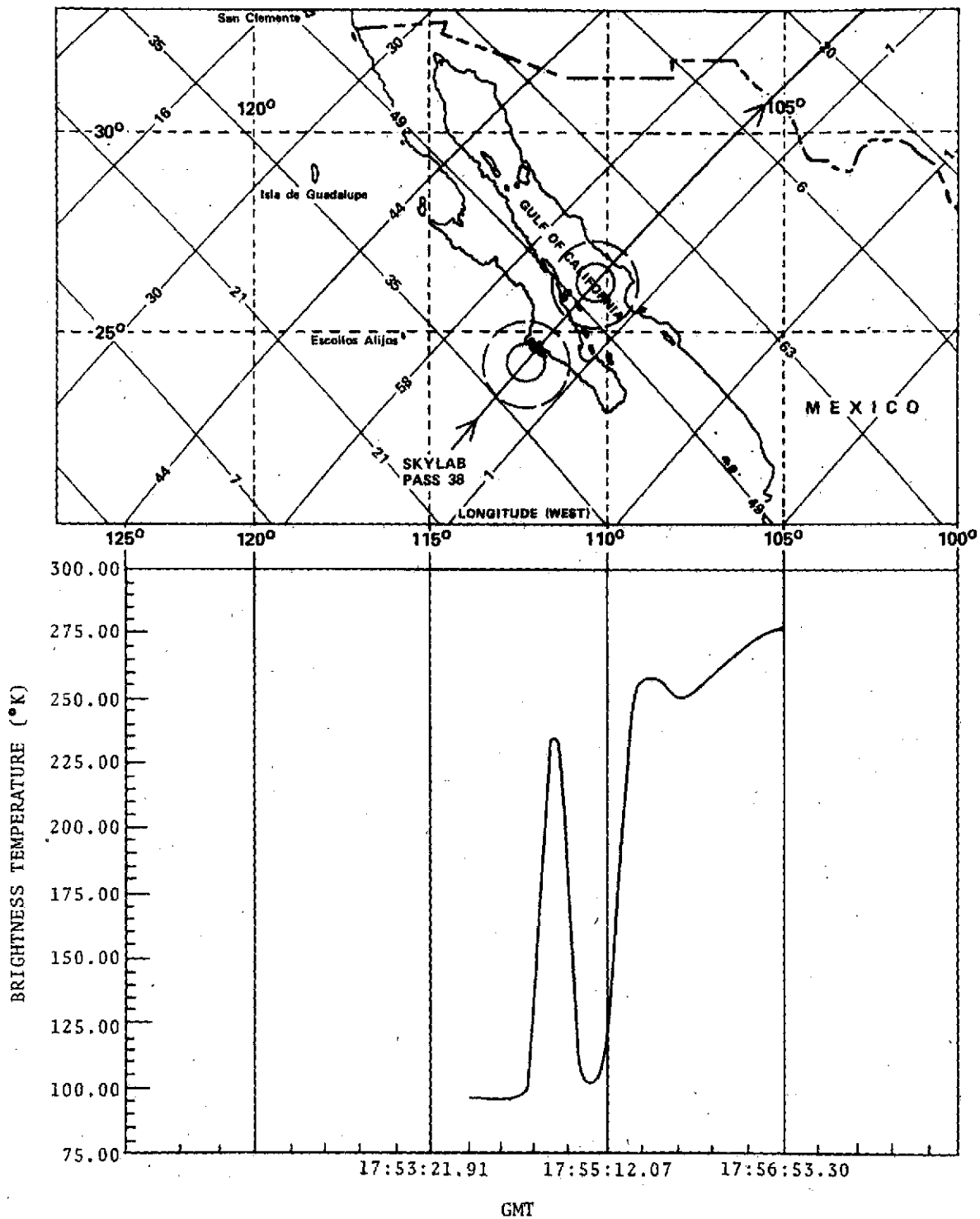Figure 7.3.2-2. — Brightness temperature versus time and position.

Figure 7.3.2-3. — Brightness temperature versus time and position.

The response of the sensor was as expected, similar to a triangular pulse with the peak occurring when the largest area of the field of view was contained by the land mass of Baja, California. The width of the pulse is proportional to the width of the land traversed along the particular ground track. The brightness temperature value of the peak of the triangle will depend on the amount of land mass within the field of view of the 3 dB points of the antenna pattern. The peak value of brightness temperature measured on Skylab pass numbers 27 and 28 are very similar, 248.1°K and 244.8°K, respectively. The lower peak value of brightness temperature acquired on Skylab pass number 38, 230.5°K, is due to less land mass within the 3 dB points of the field of view, (see Figure 7.3.2-3). Also, for Skylab pass number 38, the lower brightness temperature corresponding to the field of view over the Gulf of California is due to the fact that more of the null-to-null antenna pattern was contained in the Gulf of California than was in Skylab pass numbers 27 and 28.

Figure 7.3.2-1 (Skylab pass 27) contains the calculated brightness temperature values derived from the land/water target simulation model discussed in Section 7.2. As can be seen, there is excellent agreement between the simulated data and the actual flight data which means that no changes have occurred in the antenna since the preflight acceptance tests.

Comparison of slopes and changes in the slope of the curves in Figures 7.3.2-1, 7.3.2-2, and 7.3.2-3 reveals no noticeable change in the antenna during the time interval of approximately 7 days between Skylab pass numbers 27, 28, and 38.

Comparison of the analysis performed for the Pacific Ocean/California coastline as described in Section 7.3.1 for data acquired during SL-2 was not possible since the only pass on SL-3 over the same ground track was initiated inland from the coastline.

7.3.3 SL-4 Antenna Performance from Land/Water Interface

The flight data acquired over Baja, California, during Skylab pass numbers 81 and 82 is shown in Figures 7.3.3-1 and 7.3.3-2, respectively. An internal calibration was performed during the first part of pass 82 over the target site, thus reducing the value of the data for this application.
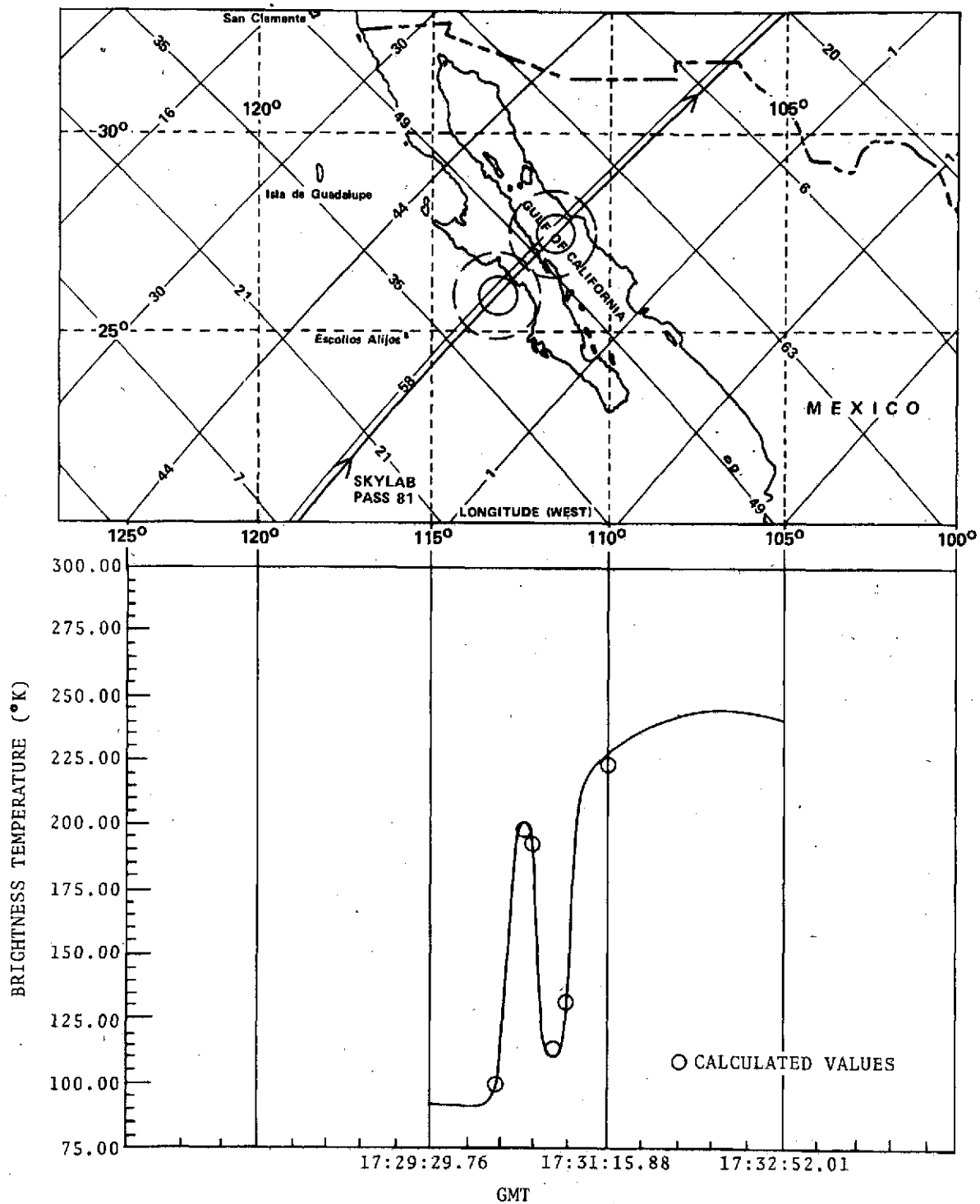
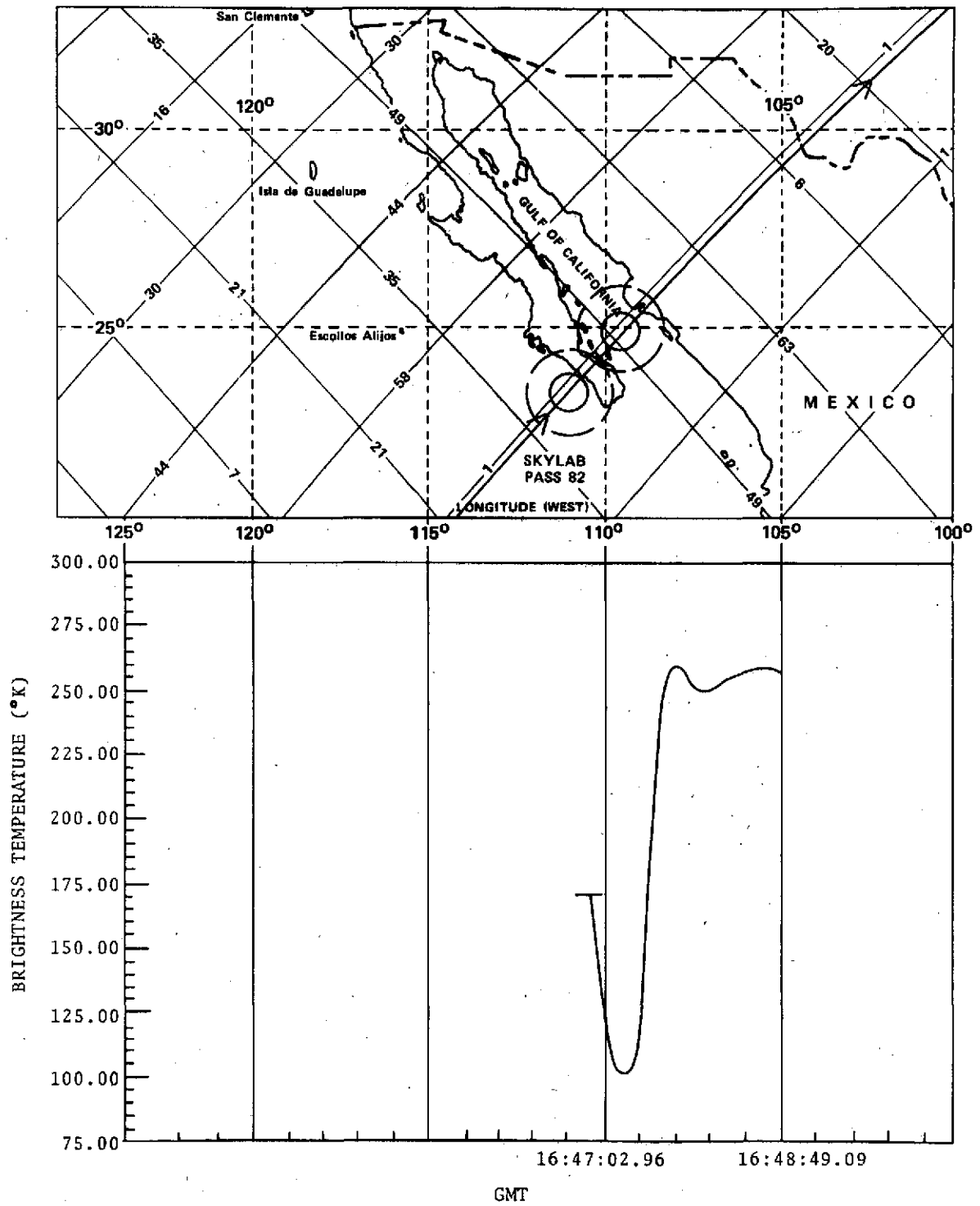Figure 7.3.3-1. — Brightness temperature versus time and position.

Figure 7.3.3-2. — Brightness temperature versus time and position.

The calculated values derived from a simulation of Skylab pass 81 target conditions are shown in Figure 7.3.3-1. Again, excellent agreement between simulated and flight data was attained indicating no change in antenna characteristics. This is further shown to be true by comparison of the slopes and slope changes between all Skylab passes over this target site.

7.4 Antenna Resolution

Utilizing the data acquired over the land/water interface of the California coastline and the fact that a y-factor measurement is performed at a rate of three samples per second, the change in brightness temperature and corresponding change in area of the field of view of the antenna will provide an estimate on antenna resolution.

The weighted brightness temperature data acquired on Skylab pass number 11 while the field of view was traversing the land/water interface of the California coastline is plotted versus time in the upper half of Figure 7.4-1. The corresponding change in land area viewed by the S194 antenna (null-to-null) was calculated and is plotted in the lower half of Figure 7.4-1 versus time. As would be expected, the greatest change in land area within the field of view of the antenna occurs at the center of the approximately circular field of view. The change in land area viewed at the trailing end of the curve in Figure 7.4-1 does not compare exactly with the change in land area viewed at the leading end of the curve. This is probably due to round-off errors in the digital integration program utilized to calculate this curve.
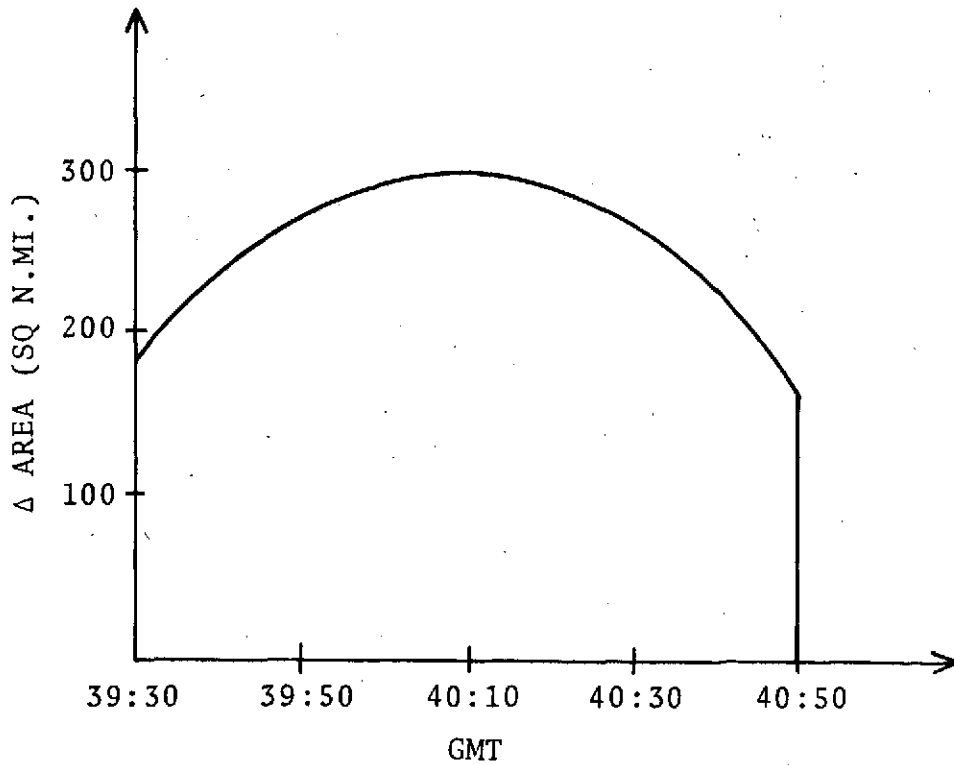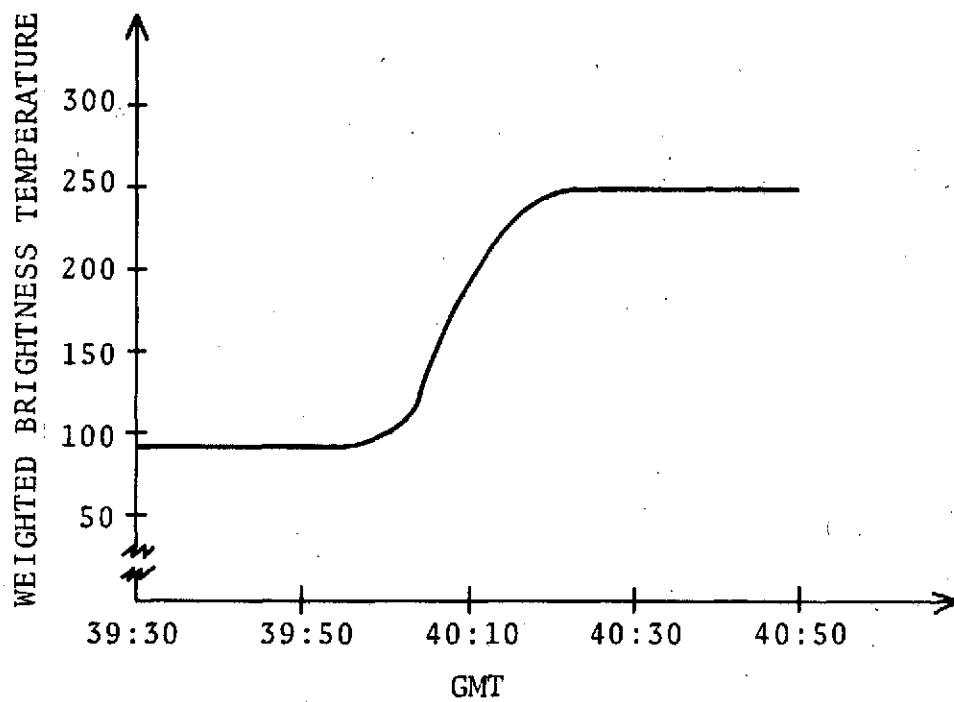
Figure 7.4-1. — Brightness temperature and Δ area versus GMT.